

# Frustrated superconductivity and sextetting order

Zhiming Pan,<sup>1,2,\*</sup> Chen Lu,<sup>2,\*</sup> Fan Yang,<sup>3,†</sup> and Congjun Wu<sup>2,1,4,5,‡</sup>

<sup>1</sup>*Institute for Theoretical Sciences, Westlake University, Hangzhou 310024, Zhejiang, China*

<sup>2</sup>*New Cornerstone Science Laboratory, Department of Physics,*

*School of Science, Westlake University, Hangzhou 310024, Zhejiang, China*

<sup>3</sup>*School of Physics, Beijing Institute of Technology, Beijing 100081, China*

<sup>4</sup>*Key Laboratory for Quantum Materials of Zhejiang Province,*

*School of Science, Westlake University, Hangzhou 310024, Zhejiang, China*

<sup>5</sup>*Institute of Natural Sciences, Westlake Institute for Advanced Study, Hangzhou 310024, Zhejiang, China*

Superconducting phase typically favors a uniform spatial distribution like ferromagnet. Nevertheless, the pair-density-wave state exhibits sign changes in the pairing order, and thus frustrations can occur in phase coherence. We propose a mechanism to the sextetting order arising from the frustrations in the phase coherence of a pair-density-wave state, whose spatial modulation manifests a vortex-antivortex honeycomb lattice. The classical ground state configurations are mapped to Baxter's three-coloring model, exhibiting a macroscopic degeneracy and extensive entropy. The phase coherence problem couples the  $U(1)$  phases and the vorticity variables together. The resultant color and phase fluctuations suppress the pair-density-wave order but maintain the sextetting order above the superconducting  $T_c$ . The  $1/3$ -fractional vortex emerges as the fundamental topological defect in the sextetting order. This novel frustrated superconductivity provides an alternative explanation for the experimental observation of fractional oscillation in  $\text{CsV}_3\text{Sb}_5$ .

## INTRODUCTION

The multi-fermion ordering has received considerable attention in a wide range of research fields in modern physics. Inside a heavy nucleus, the alpha-particle-like quartetting instability involving two protons and two neutrons competes with the deuteron-like instability of pairing between one proton and one neutron [1]. Its many-body version has been investigated in the 1D spin- $\frac{3}{2}$  ultra-cold fermion system via bosonization, revealing the Ising-dual relation between these two instabilities [2]. In the context of superconductivity (SC) in electron systems, the multi-fermion ordering, quartetting or sextetting, can emerge as a vestigial secondary order of the charge- $2e$  Cooper pairing SC above the superconducting critical temperature  $T_c$ , often termed as the so-called charge- $4e$ , or, charge- $6e$  SC states [3–16].

The quartetting or sextetting states can appear as a consequence of melting the pair-density-wave (PDW) state, i.e., the superconducting pairing orders  $\Delta_{\mathbf{Q}}$  carrying finite momenta [6–8]. A PDW state can exhibit multiple incommensurate wave vectors  $\mathbf{Q}$ , and the incommensurabilities render the relative phases of the translational degree of freedom gapless. There exist topological defects related to the translational phase, and the system undergoes a Kosterlitz-Thouless (KT) type transition [17] as temperature increases. The PDW superconducting order disappears above a critical temperature  $T_c$  due to the strong fluctuations in the relative phase channels, nevertheless, the overall phase remains ordered, leading to the quartetting or sextetting state [6–8].

Here we propose an alternative mechanism based on the frustrations of the superconducting phase coherence, which naturally leads to the sextetting order. Usually the

frustrated systems are characterized by the macroscopic degeneracy of ground-state configurations at the classic level [18, 19]. The three-coloring model on the honeycomb lattice [20] is a celebrated example, which applies to various frustrated systems including classical antiferromagnets [21], Josephson junction arrays [22, 23], orbital-active materials [24–26], and other systems [11, 27, 28]. Each bond of the honeycomb lattice is painted by one of the three colors  $\mathbf{R}$ (red),  $\mathbf{G}$ (green),  $\mathbf{B}$ (blue) under the so-called “color constraint” that three bonds connected to the same vertex are painted by different colors. The classical ground-state configurations exhibit a macroscopic degeneracy, leading to an extensive entropy of  $0.38k_B$  per hexagon [20]. The strong frustrations kill the order of the single color variable, but a combined three-color order could survive. This frustration mechanism has also been extended to the four-coloring model on the three-dimensional diamond lattice [29], which exhibits the dipolar correlation characterized by a cubic power decay  $1/R^3$ .

In this article, we investigate the sextetting order in the superconductivity via frustrations to the PDW order. The corresponding superconducting phase coherence problem is mapped to the three-coloring model, exhibiting macroscopic degeneracy arising from color configurations. The low-energy degrees of freedom encompass the local pairing-phases coupled to the vorticity variables. Monte-Carlo simulations are performed to obtain the phase diagram, showing the competition between the Cooper pairing and sextetting order. The entropy associated with the color configurations dominates, leading to the sextetting state at a higher temperature before the system enters the completely disordered regime. Moreover, the sextetting order manifests  $1/3$ -fractional vortex, providing an alternative mechanism to the fractional flux

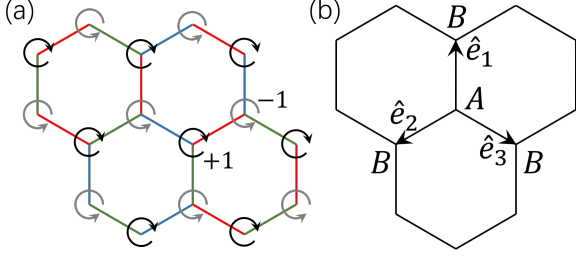


FIG. 1. (a). A honeycomb lattice of vortices/antivortices. Here, an AFM-like vortex-antivortex pattern satisfying the three-color constraint is shown. The superconducting phases along three bond directions can take values of  $0, \frac{2}{3}\pi, \frac{4}{3}\pi$  denoted by three colors **R, G, B**. (b). The honeycomb lattice with *A, B* sublattice. The three bond directions are denoted as  $\hat{e}_\nu$  ( $\nu = 1, 2, 3$ ).

oscillations.

### VORTEX-ANTIVORTEX HONEYCOMB LATTICE

Frustrated superconductivity emerges from phase coherence of a vortex-antivortex honeycomb lattice. The vortex lattice model could be realized through Josephson junction arrays[22], *p*-orbital unconventional superfluidity[30] or PDW state[8, 31]. The cores of single vortices/anti-vortices are located at the sites of the honeycomb lattice, with phase winding  $\pm 2\pi$  around it. A pair of neighboring single vortices couple with each other through Josephson coupling and inter-vortex coupling. In the ground state, all the vortices and antivortices exhibit phase coherence, leading to unconventional superconductivity with simultaneously time-reversal symmetry breaking [30]. A typical vortex-antivortex pattern with alternating vortices/anti-vortices is illustrated in Fig. 1(a). Furthermore, the superconducting phase order induced by a fixed coherent pattern of vortices and anti-vortices can display spatial modulation, giving rise to the pair-density-wave order.

The vortex-antivortex model can be mapped to the three-coloring problem on the honeycomb lattice [22, 30]. (Its generalization to the four-coloring problem in the diamond lattice was done by Chern and one of the authors [29].) The superconducting phase winds  $\pm 2\pi$  around a site *j* of the honeycomb lattice, depending on whether a vortex or antivortex is located at that site. Each site is connected to its three nearest neighbors and the angles between two bond directions are all  $120^\circ$ . Hence, to minimize the phase difference across each bond, without loss of generality, we can assign three colors **R, G, B** corresponding to the phases  $1, e^{i\frac{2}{3}\pi}, e^{i\frac{4}{3}\pi}$ , respectively, and paint each bond according to this color constraint. The clockwise or anticlockwise ordering of the colors **R, G, B** defines the chirality  $\tau_j = \pm 1$ , or, the vorticity. Under

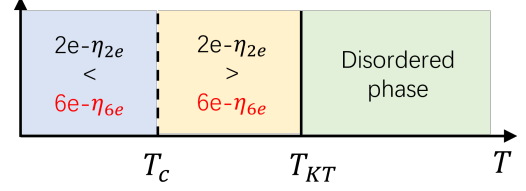


FIG. 2. A schematic phase diagram of the effective model in Eq. (1). At low temperatures  $T < T_c$ ,  $2e$  quasi-long-range order (QLRO) dominates ( $\eta_{2e} < \eta_{6e}$ ), while at intermediate temperatures ( $T_c < T < T_{KT}$ ),  $6e$  QLRO takes precedence. Above the KT temperature  $T_{KT}$  of the U(1) phase, the system is in the disordered phase.

time-reversal transform, the vorticities are flipped. If only considering the color frustration effect, the charge- $2e$  correlation of the phases exhibits power-law decay,  $G_{2e}(r) \sim r^{-4/3}$  [21].

To fully describe the phase coherence of the superconducting state, it is essential to account for U(1) phase fluctuations. For later convenience, the following convention is employed: The honeycomb lattice system is divided into two sublattices *A* and *B*, as depicted in Fig. 1(b). Consider a site *j* belonging to sublattice *A*. It emits three bonds denoted as  $\hat{e}_\nu$  whose azimuthal angles are  $90^\circ, 210^\circ, 330^\circ$  for bond index  $\nu = 1, 2, 3$ , respectively. The superconducting phase along the  $\hat{e}_1$  direction is denoted as  $\theta_j$ . On the other hand, for a site *k* belonging to sublattice *B*, its superconducting phase along  $-\hat{e}_1$  direction is set as  $\theta_k$ . Then around any site *j*, the superconducting phase along the bond  $\nu$  is represented as  $\theta_j + \tau_j \phi_\nu$ , where  $\phi_\nu = 0, \frac{2}{3}\pi, \frac{4}{3}\pi$  for  $\nu = 1, 2, 3$ , respectively. Then the effective Hamiltonian reads [30],

$$H = -J \sum_{j \in A, \nu} \cos [\theta_j - \theta_k + (\tau_j - \tau_k) \phi_\nu] - J_2 \sum_{j \in A, \nu} \cos [\theta_j - \theta_k + (\tau_j - \tau_k) \phi_\nu + \frac{\pi}{2} (\tau_j + \tau_k)], \quad (1)$$

where the summation over *j* is only carried on sublattice *A*, and *k* belongs to sublattice *B* along the bond direction of  $\hat{e}_\nu$ . The *J*-term represents the nearest-neighbor Josephson coupling, whose dependence on the bond geometry can be viewed as a vector potential  $A_{jk} = (\tau_j - \tau_k) \phi_\nu$ . The *J*<sub>2</sub>-term describes the coupling between nearest vortices in the perpendicular direction[30]. A little *J*<sub>2</sub>-term could fix the vortex configuration into a specific antiferromagnetic (AFM) like pattern, where nearest neighbours exhibit opposite vorticities as depicted in Fig. 1(a).

If the temperature *T* is lower than the KT transition temperature  $T_{KT}$  of the U(1) phase  $\theta_i$ , but is still high enough such that the long-range inter-vortex interactions (e.g., *J*<sub>2</sub>-term) can be neglected, then the entropy of the color configurations dominates. As a result, there is no long-range pairing order, but the cube of the pairing or-

der is long-range ordered since color variables  $1, \omega, \omega^2$  are cubic roots of 1 with  $\omega = e^{i\frac{2}{3}\pi}$ . This manifests as the sextetting superconductivity. As the temperature is lowered enough, the inter-vortex interactions will lift the degeneracy among different vortex configurations. The ordered PDW configuration emerges, resulting in the transition to the charge- $2e$  superconducting state. A schematic phase diagram of the system is summarised as in Fig. 2.

## NUMERICAL SIMULATION

Monte-Carlo simulations are performed to simulate the Hamiltonian of Eq. (1). Importantly, the update method depends on the relevant temperature regime. Similar situation appears in many frustrated systems, e.g., in the Ref. [27], due to the macroscopic degeneracy at low temperature. We will follow the same inspiration in Ref. [27], separating the temperature into lower and higher regime. Above the KT temperature of the U(1) phase  $\theta_i$ ,  $1/3$ -fractional vortices proliferate and the U(1) phase coherence is destroyed. The color configurations are disordered. The system exhibits the disordered phase, where the U(1) phase correlation, or charge- $2e$  correlation,  $\langle e^{i\theta_j} e^{-i\theta_k} \rangle$  between two sites  $j, k$  decays exponentially as the relative distance increases. The local update of the chiralities and phase variables is sufficient to handle the disordered phase. As temperature decreases, the vorticity configuration tends to satisfy the color constraint and the local update breaks down [27]. Alternatively, we apply the loop update where the vorticity configuration keeps the color constraint in each update step. The U(1) phase variables are updated simultaneously according to the vorticity configuration. (see App.A for the details).

The simulation of the critical exponents for the superconducting phase correlations in the low temperature regime is summarized in Fig. 3(a), which shows two competing phases: lower temperature charge- $2e$  superconductivity, and higher temperature charge- $6e$  dominated phase. The charge- $2e$  and charge- $6e$  correlations are characterized by the quasi-long-range ordering (QLRO) of the relevant phase correlations defined as  $\langle e^{i\theta_j} e^{-i\theta_k} \rangle \sim r^{-\eta_{2e}}$  and  $\langle e^{3i\theta_j} e^{-3i\theta_k} \rangle \sim r^{-\eta_{6e}}$ , where  $r$  is the distance between the two sites  $j, k$ . Here,  $\eta_{2e}$  and  $\eta_{6e}$  are power-law decay exponents for the charge- $2e$  and  $6e$  correlations. For comparison, the critical exponent  $\eta_{4e}$  of the  $4e$ -correlation,  $\langle e^{2i\theta_j} e^{-2i\theta_k} \rangle \sim r^{-\eta_{4e}}$ , is also deduced from the numerical estimation.

The three critical exponents fit well with the following relations,  $\eta_{2e} = \eta_c + \eta_{6e}/9$  and  $\eta_{4e} = \eta_c + 4\eta_{6e}/9$ . Here,  $\eta_c$  represents the contribution of color frustration in the vorticity correlation, which does not contribute to the charge- $6e$  correlation. At low enough temperature, the vortex configuration is fixed with  $\eta_c = 0$  and the critical exponents are only related to the QLRO of the

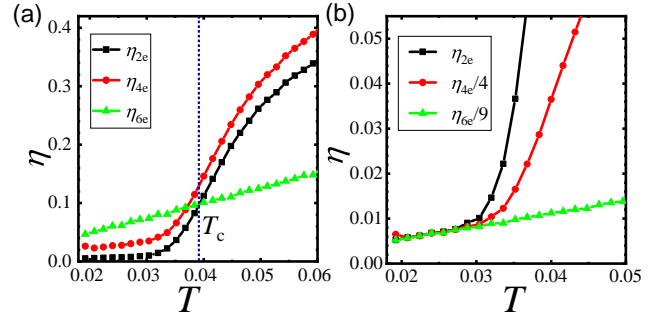


FIG. 3. (a). Critical exponents  $\eta$  for  $2e$ -,  $4e$ - and  $6e$ -correlations evaluated from model (1) at  $J = 1$  and  $J_2 = 0.01$  in the temperature regime well below  $T_{KT}$ . At lower temperature below  $T_c$ , charge- $2e$  correlation exhibits greater strength compared to the charge- $6e$  correlation ( $\eta_{2e} < \eta_{6e}$ ). Color frustration emerges at higher temperature and above  $T_c$ , charge- $6e$  correlation dominates. (b).  $\eta_{2e}, \eta_{4e}/4$  and  $\eta_{6e}/9$  are presented for comparison. At low enough temperature ( $T \lesssim 0.03$ ), these quantities converge to nearly identical values, i.e., color configuration is pinned down in this regime.

U(1) phase variables,  $\eta_{2e} = \eta_{4e}/4 = \eta_{6e}/9$ , as depicted in Fig. 3(b). The low-temperature regime is characterized by the dominance of charge- $2e$  behavior ( $\eta_{2e} < \eta_{6e}$ ). As temperature increases, color frustration begins to manifest, encoding in a finite  $\eta_c$ . Above the critical temperature  $T_c$ , the entropy associated with color configurations takes precedence over the energy cost arising from the  $J_2$ -term and the charge- $2e$  correlation is suppressed. The charge- $6e$  behavior dominates over the charge- $2e$  correlation, as evidenced by the relationship  $\eta_{6e} < \eta_{2e}$ . Moreover, the estimated color correlation  $\eta_c$  is much smaller than  $4/3$  for the pure three-color model [21]. Different color configurations have unequal weights around the staggered AFM-like vortex pattern preferred by the  $J_2$  term.

Above the KT temperature  $T_{KT}$  of the U(1) phase variables  $\theta_i$ , both charge- $2e$  and  $6e$  correlations exhibit exponential decay, leading the system into a disordered phase. The color configuration also becomes disordered and a local update proves sufficient for estimating correlation behavior above  $T_{KT}$ . The numerical simulation confirms the exponentially decay behavior of the correlations in this regime. However, due to limitations in Monte Carlo simulation, as mentioned earlier, precise determination of the KT temperature is not feasible. As the temperature decreases from high to the critical temperature  $T_{KT}$ , the effectiveness of local updates gradually diminishes, reflected in rapidly increasing acceptance rates and computation times. The temperature at which the local updates become ineffective is approximately around 0.13, establishing an upper bound for  $T_{KT}$ . This kind of numerical difficulty is common in frustrated system, e.g., happening in Ref. [27]. More advanced method is necessary for completely simulating the problem, which is

leaving for further works.

The preceding analysis focuses on the inherently two-dimensional system, where charge- $2e$  and charge- $6e$  correlations exhibit only quasi-long-range order. In the real materials, it is natural that the system comprises layered 2D lattices, thereby forming a quasi-two-dimensional model. The inter-layer couplings between the 2D layers could enhance the QLRO, leading to the stabilization of a true long-range order of either charge- $2e$  type (for  $\eta_{2e} < \eta_{6e}$  regime) or charge- $6e$  type (for  $\eta_{6e} < \eta_{2e}$  regime) at low temperature.

The  $\frac{1}{3}$ -fractional flux can emerge above the  $T_c$  of the PDW order due to fluctuations of the vorticity variables [22, 30]. Around each hexagonal vortice/antivortice plaquette  $h$ , its total vorticity is defined as  $\Phi_h = \frac{1}{3} \sum_{i \in h} \tau_i$ . For a configuration under the color constraint, the vorticity around a plaquette takes values of  $0, \pm 2$ . A fundamental topological defect exhibits a domain wall which is a string of bonds with mismatched color variables. The plaquette containing the ending point of a domain wall is the core of a  $\frac{1}{3}$ -vortex, or, a  $\frac{1}{3}$ -antivortex. Around the vortex core, the superconducting phase winding equals to  $\pm \frac{2}{3}\pi$ . An external magnetic flux at one third of the value of the fundamental flux generates a  $\frac{1}{3}$ -vortex such that the superconducting phase across each bond remain matched. Consequently, the free energy will show periodic modulation under the flux change of

$$\Phi_{6e} = \frac{hc}{6e}, \quad (2)$$

respecting the charge- $6e$  QLRO and  $1/3$ -fractional flux.

### PDW STATES

PDW states exhibiting spatial modulation of the pairing order have been proposed in the FFLO states [32, 33]. The vortex-antivortex model provides a platform for realizing the PDW state as its ground state. In the hexagonal crystal system, PDW state can manifest 6 commensurate wave vectors denoted as  $\pm \mathbf{Q}_i$  ( $i = 1, 2, 3$ ). The spatial distribution of PDW order parameter is represented as [8],

$$\Delta(\mathbf{r}) = \sum_i (\Delta_{\mathbf{Q}_i} e^{i\mathbf{Q}_i \cdot \mathbf{r}} + \Delta_{-\mathbf{Q}_i} e^{-i\mathbf{Q}_i \cdot \mathbf{r}}), \quad (3)$$

where the gap functions  $\Delta_{\pm \mathbf{Q}_i}$  ( $i = 1, 2, 3$ ) carry nonzero mass-of-center momentum  $\pm \mathbf{Q}_i$ , respectively. The ground state configuration can be determined by the Ginzburg-Landau free energy [8], presenting several possibilities depending on the microscopic details of the relevant model.

For the previously considered AFM-like vortex-antivortex pattern, it corresponds to an inversion symmetric breaking PDW state with only three wavevectors

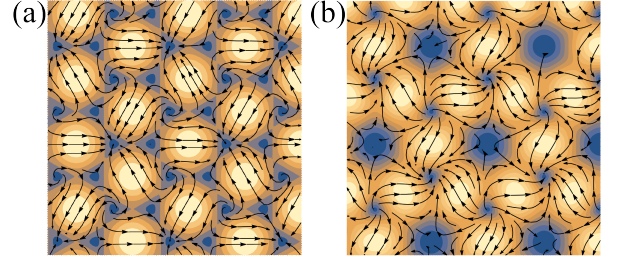


FIG. 4. The vortex-antivortex lattice pattern of the PDW state for the (a)  $3Q$  state and (b)  $6Q$  state. In the  $3Q$  state, single vortices and antivortices form a honeycomb lattice. In the  $6Q$  state, single vortices (or antivortices) form a honeycomb lattice with double antivortices (or vortices) in the centers of the hexagons.

$\mathbf{Q}_1, \mathbf{Q}_2$  and  $\mathbf{Q}_3$ . The superconducting order parameter is given by

$$\Delta_{3Q}(\mathbf{r}) = \Delta_{3Q} (e^{i\mathbf{Q}_1 \cdot \mathbf{r}} + e^{i\theta_2 + i\mathbf{Q}_2 \cdot \mathbf{r}} + e^{i\theta_3 + i\mathbf{Q}_3 \cdot \mathbf{r}}), \quad (4)$$

with relative phases  $\theta_2, \theta_3$  between the three PDW components. This  $3Q$  state forms a honeycomb lattice with alternating vortices/antivortices as illustrated in Fig. 4(a) [8]. On the other hand, when inversion symmetry is preserved, the  $6Q$  PDW order parameter exhibits all the six momenta and a typical chiral PDW pattern is depicted in Fig. 4(b) [8, 31], where vortices or antivortices with higher vorticity appear. The  $3Q$ -state with AFM-like vortex/antivortex lattice pattern could be more energetically favorable than the  $6Q$ -state. Notice that previous mechanism of frustrated superconductivity could similarly occur in the  $6Q$ -state, where the honeycomb lattice is formed from single vortices or antivortices.

In the STM experimental detection of the PDW state, the local density of state (LDOS) could exhibit extra spatial modulation resulting from the PDW state [34–41]. When the uniform SC  $\Delta_0$  coexists and dominates, the strong peaks shown in the Fourier transform of LDOS corresponds to the PDW wavevectors directly. The uniform SC component couples to a particular PDW component  $\Delta_{\mathbf{Q}}$ , contributing to a spatial modulation component  $N_{\mathbf{Q}}(\mathbf{r})$  in LDOS to the lowest order,

$$N_{\mathbf{Q}}(\mathbf{r}) \propto \Delta_0^* \Delta_{\mathbf{Q}} e^{i\mathbf{Q} \cdot \mathbf{r}} + \Delta_0 \Delta_{\mathbf{Q}}^* e^{-i\mathbf{Q} \cdot \mathbf{r}}. \quad (5)$$

The LDOS measurement from STM experiment can not distinguish the  $3Q$  PDW state and  $6Q$  PDW state up to this order, since both of them would exhibit six peaks in the Fourier spectrum of LDOS.

The difference between the LDOS patterns of  $3Q$  and  $6Q$  state arise from the couplings among PDW components. A pair of two PDW components,  $\Delta_{\mathbf{Q}_i}, \Delta_{\mathbf{Q}_j}$ , will contribute to the LDOS,

$$N_{\mathbf{Q}_i - \mathbf{Q}_j}(\mathbf{r}) \propto \Delta_{\mathbf{Q}_i}^* \Delta_{\mathbf{Q}_j} e^{i(\mathbf{Q}_i - \mathbf{Q}_j) \cdot \mathbf{r}} + \text{h.c.} \quad (6)$$

For the  $3Q$  state, LDOS pattern exhibits peaks correspond to the wavevector  $\pm(\mathbf{Q}_i - \mathbf{Q}_j)$  with  $i \neq j = 1, 2, 3$ .

For the  $6Q$  state, several extra peaks  $\pm 2\mathbf{Q}_i$  ( $i = 1, 2, 3$ ) different from  $3Q$  state appear. Such difference could be helpful to distinguish these two PDW states.

## DISCUSSIONS

Recently, superconductivity of the Kagome material  $\text{AV}_3\text{Sb}_5$  ( $A=\text{K,Rb,Cs}$ ) has been observed [42–44]. A  $\frac{4}{3} \times \frac{4}{3}$  bidirectional spatial modulation of the superconducting gap function is observed [40] in the low-temperature superconducting state on top of a  $2 \times 2$  charge-density-wave (CDW) normal-state background [31, 45–48]. This superconducting state is suggested to be a chiral PDW SC which breaks the time-reversal symmetry spontaneously [31, 40]. However, as described previously, it may not be easy to distinguish the  $3Q$ -PDW and  $6Q$ -PDW order when only six peaks are clearly seen in the experiment [40].

A particularly interesting experimental progress on the  $\text{CsV}_3\text{Sb}_5$  superconductor is the detection of the  $hc/(6e)$  magneto-resistance oscillation period in the Little-Parks experiment above  $T_c$ , one third of the conventional Little-Parks oscillation [49], which has aroused considerable interests [31, 50–53]. The above mechanism to the charge- $6e$  state based on the frustrations of the PDW order may be applied to this fractional  $hc/(6e)$  oscillation. The experiment set up is a thin  $\text{CsV}_3\text{Sb}_5$  flake with a hole forming a mesoscopic ring. Below the  $T_c$  of the PDW order, an external magnetic flux going through the hole generates an integer vorticity, accounting for the conventional  $hc/2e$  oscillation. As increasing temperature, frustrations suppress the charge- $2e$  PDW order but favor the charge- $6e$  order. An external magnetic flux of  $n$  times of  $hc/6e$  can generate the  $n/3$  fractional vorticity, with the core pinned inside the hole, which gives rise to the  $hc/6e$  type quantum oscillations.

The above idea of frustrated superfluidity can also be extended to three dimensions. The three-coloring model is generalized to the 4-coloring model defined on a diamond lattice, and the color constraint is updated as that all the four bonds connected to a lattice site should be painted by the  $\mathbf{R}, \mathbf{G}, \mathbf{B}, \mathbf{Y}$  colors without repetition [29]. The  $\mathbf{R}, \mathbf{G}, \mathbf{B}, \mathbf{Y}$  colors represent the quartic unit roots  $1, i, -1, -i$  respectively. The frustration therein could favor a charge- $8e$  state.

## CONCLUSIONS

We study the phase frustrations in the vortex-antivortex model on the honeycomb lattice by mapping its superconducting phase coherence problem to the three coloring model. The fundamental degrees of freedom are described by the  $U(1)$  phase coupled to the discrete vorticity variables. The classical ground states, subject to

the color constraints, exhibit a macroscopic degeneracy in terms of coloring patterns. The inclusion of inter-vortex coupling results in a phase coherent ground state pattern that naturally realizes the pair-density-wave state. Above the superconducting transition temperature ( $T_c$ ), charge- $6e$  order prevails over the Cooper charge- $2e$  order, persisting until the system enters a disordered regime. Such behavior is further numerically verified through Monte Carlo simulations. The fundamental topological defects are  $\pm \frac{1}{3}$  vortices, which can lead to the  $hc/6e$  flux modulations. Our findings establish possible connections to the recent quantum oscillation experiments on the Kagome superconductor  $\text{CsV}_3\text{Sb}_5$  [49].

**Acknowledgments** We are grateful to the stimulating discussions with Shaokai Jian and Zheng Yan. C.W. is supported by the National Natural Science Foundation of China under the Grants No. 12234016 and No. 12174317. This work has been supported by the New Cornerstone Science Foundation. F.Y. is supported by the National Natural Science Foundation of China under the Grants No. 12074031. C.L. is supported by the National Natural Science Foundation of China under the Grants No. 12304180.

---

\* These two authors contributed equally to this work.

† yangfan\_blg@bit.edu.cn

‡ wucongjun@westlake.edu.cn

- [1] G. Röpke, A. Schnell, P. Schuck, and P. Nozieres, *Physical review letters* **80**, 3177 (1998).
- [2] C. Wu, *Physical review letters* **95**, 266404 (2005).
- [3] S. Korshunov, *Zh. Eksp. Teor. Fiz* **89**, 531 (1985).
- [4] S. Kivelson, V. Emery, and H. Lin, *Physical Review B* **42**, 6523 (1990).
- [5] A. Aligia, A. P. Kampf, and J. Mannhart, *Physical review letters* **94**, 247004 (2005).
- [6] D. Agterberg and H. Tsunetsugu, *Nature Physics* **4**, 639 (2008).
- [7] E. Berg, E. Fradkin, and S. A. Kivelson, *Nature Physics* **5**, 830 (2009).
- [8] D. F. Agterberg, M. Geracie, and H. Tsunetsugu, *Phys. Rev. B* **84**, 014513 (2011).
- [9] W.-H. Ko, P. A. Lee, and X.-G. Wen, *Physical Review B* **79**, 214502 (2009).
- [10] E. V. Herland, E. Babaev, and A. Sudbø, *Physical Review B* **82**, 134511 (2010).
- [11] Y.-Z. You, Z. Chen, X.-Q. Sun, and H. Zhai, *Phys. Rev. Lett.* **109**, 265302 (2012).
- [12] Y.-F. Jiang, Z.-X. Li, S. A. Kivelson, and H. Yao, *Physical Review B* **95**, 241103 (2017).
- [13] M. Zeng, L.-H. Hu, H.-Y. Hu, Y.-Z. You, and C. Wu, *arXiv preprint arXiv:2102.06158* (2021).
- [14] R. M. Fernandes and L. Fu, *Physical review letters* **127**, 047001 (2021).
- [15] S.-K. Jian, Y. Huang, and H. Yao, *Physical Review Letters* **127**, 227001 (2021).
- [16] G. Volovik, *arXiv preprint arXiv:2312.09435* (2023).
- [17] J. M. Kosterlitz and D. J. Thouless, in *Basic Notions Of*

*Condensed Matter Physics* (CRC Press, 2018) pp. 493–515.

- [18] R. Moessner and A. P. Ramirez, *Phys. Today* **59**, 24 (2006).
- [19] L. Balents, *Nature* **464**, 199 (2010).
- [20] R. Baxter, *Journal of Mathematical Physics* **11**, 784 (1970).
- [21] D. A. Huse and A. D. Rutenberg, *Phys. Rev. B* **45**, 7536 (1992).
- [22] J. E. Moore and D.-H. Lee, *Phys. Rev. B* **69**, 104511 (2004).
- [23] C. Castelnovo, P. Pujol, and C. Chamon, *Physical Review B* **69**, 104529 (2004).
- [24] C. Wu, D. Bergman, L. Balents, and S. Das Sarma, *Phys. Rev. Lett.* **99**, 070401 (2007).
- [25] C. Wu, *Phys. Rev. Lett.* **100**, 200406 (2008).
- [26] C. Wu and S. Das Sarma, *Phys. Rev. B* **77**, 235107 (2008).
- [27] G.-W. Chern, C. Reichhardt, and C. O. Reichhardt, *Physical Review E* **87**, 062305 (2013).
- [28] B. Chakraborty, D. Das, and J. Kondev, *The European Physical Journal E* **9**, 227 (2002).
- [29] G.-W. Chern and C. Wu, *Phys. Rev. Lett.* **112**, 020601 (2014).
- [30] C. Wu, *Modern Physics Letters B* **23**, 1 (2009).
- [31] S. Zhou and Z. Wang, *Nature Communications* **13**, 1 (2022).
- [32] P. Fulde and R. A. Ferrell, *Phys. Rev.* **135**, A550 (1964).
- [33] A. Larkin and I. Ovchinnikov, *Soviet Physics-JETP* **20**, 762 (1965).
- [34] M. Hamidian, S. Edkins, S. H. Joo, A. Kostin, H. Eisaki, S. Uchida, M. Lawler, E.-A. Kim, A. Mackenzie, K. Fujita, *et al.*, *Nature* **532**, 343 (2016).
- [35] Z. Dai, Y.-H. Zhang, T. Senthil, and P. A. Lee, *Physical Review B* **97**, 174511 (2018).
- [36] Y. Wang, S. D. Edkins, M. H. Hamidian, J. S. Davis, E. Fradkin, and S. A. Kivelson, *Physical Review B* **97**, 174510 (2018).
- [37] S. D. Edkins, A. Kostin, K. Fujita, A. P. Mackenzie, H. Eisaki, S. Uchida, S. Sachdev, M. J. Lawler, E.-A. Kim, J. Séamus Davis, *et al.*, *Science* **364**, 976 (2019).
- [38] Z. Du, H. Li, S. H. Joo, E. P. Donoway, J. Lee, J. S. Davis, G. Gu, P. D. Johnson, and K. Fujita, *Nature* **580**, 65 (2020).
- [39] X. Liu, Y. X. Chong, R. Sharma, and J. S. Davis, *Science* **372**, 1447 (2021).
- [40] H. Chen, H. Yang, B. Hu, Z. Zhao, J. Yuan, Y. Xing, G. Qian, Z. Huang, G. Li, Y. Ye, *et al.*, *Nature* **599**, 222 (2021).
- [41] Q. Gu, J. P. Carroll, S. Wang, S. Ran, C. Broyles, H. Siddiquee, N. P. Butch, S. R. Saha, J. Paglione, J. S. Davis, *et al.*, *Nature* **618**, 921 (2023).
- [42] B. R. Ortiz, L. C. Gomes, J. R. Morey, M. Winiarski, M. Bordelon, J. S. Mangum, I. W. H. Oswald, J. A. Rodriguez-Rivera, J. R. Neilson, S. D. Wilson, E. Ertekin, T. M. McQueen, and E. S. Toberer, *Phys. Rev. Materials* **3**, 094407 (2019).
- [43] B. R. Ortiz, S. M. L. Teicher, Y. Hu, J. L. Zuo, P. M. Sarte, E. C. Schueller, A. M. M. Abeykoon, M. J. Krogstad, S. Rosenkranz, R. Osborn, R. Seshadri, L. Balents, J. He, and S. D. Wilson, *Phys. Rev. Lett.* **125**, 247002 (2020).
- [44] B. R. Ortiz, P. M. Sarte, E. M. Kenney, M. J. Graf, S. M. L. Teicher, R. Seshadri, and S. D. Wilson, *Phys. Rev. Materials* **5**, 034801 (2021).
- [45] Z. Wang, Y.-X. Jiang, J.-X. Yin, Y. Li, G.-Y. Wang, H.-L. Huang, S. Shao, J. Liu, P. Zhu, N. Shumiya, M. S. Hossain, H. Liu, Y. Shi, J. Duan, X. Li, G. Chang, P. Dai, Z. Ye, G. Xu, Y. Wang, H. Zheng, J. Jia, M. Z. Hasan, and Y. Yao, *Phys. Rev. B* **104**, 075148 (2021).
- [46] Y.-X. Jiang, J.-X. Yin, M. M. Denner, N. Shumiya, B. R. Ortiz, G. Xu, Z. Guguchia, J. He, M. S. Hossain, X. Liu, *et al.*, *Nature Materials* **20**, 1353 (2021).
- [47] Z. Liang, X. Hou, F. Zhang, W. Ma, P. Wu, Z. Zhang, F. Yu, J.-J. Ying, K. Jiang, L. Shan, Z. Wang, and X.-H. Chen, *Phys. Rev. X* **11**, 031026 (2021).
- [48] D. Song, L. Zheng, F. Yu, J. Li, L. Nie, M. Shan, D. Zhao, S. Li, B. Kang, Z. Wu, *et al.*, *Science China Physics, Mechanics & Astronomy* **65**, 247462 (2022).
- [49] J. Ge, P. Wang, Y. Xing, Q. Yin, H. Lei, Z. Wang, and J. Wang, *arXiv preprint arXiv:2201.10352* (2022).
- [50] L.-F. Zhang, Z. Wang, and X. Hu, *arXiv preprint arXiv:2205.08732* (2022).
- [51] J. H. Han and P. A. Lee, *Physical Review B* **106**, 184515 (2022).
- [52] Y. Yu, *arXiv preprint arXiv:2210.00023* (2022).
- [53] J.-T. Jin, K. Jiang, H. Yao, and Y. Zhou, *Phys. Rev. Lett.* **129**, 167001 (2022).

## APPENDIX A

In this appendix, we provide a detailed explanation of the combined loop update method employed in low-temperature Monte Carlo simulations. At exceedingly low temperatures, the system primarily manifests states within the three-color subspace, adhering to color configurations subjected to color constraints. To effectively capture the system's behavior in such conditions, we would confine the simulation to the three-color subspace in this temperature regime.

For the implementation of the combined loop update method, we initially define loops within the three-color subspace. These loops are generated by traversing a path with two alternating colors, such as  $RGRG\cdots$ , as depicted in Fig. 5(b). Importantly, the interchange of the two colors along the loop does not violate the three-color constraint. In the loop update, a specific loop is selected, and colors along its path are interchanged, effectively flipping the chiralities along the loop.

Simultaneous updates of the  $U(1)$  phases are also necessary for the sufficiency of the simulation. During the loop update, the chiralities along the loop  $L$  are flipped, and the local  $U(1)$  phases  $\theta_i (i \in L)$  are altered concurrently. It is crucial to note that each site  $i \in L$  within the loop possesses one external bond that is not part of the loop, featuring a phase coupling denoted as  $\phi_{i,\text{out}}$  at the bond. The transformation of  $\theta_i (i \in L)$  under the update is determined while keeping the external phase  $\varphi_{i,\text{out}}$  fixed,

$$\varphi_{i,\nu=\text{out}} = \theta_i^{(0)} + \phi_{i,\text{out}}\tau_i^{(0)} = \theta_i^{(1)} + \phi_{i,\text{out}}\tau_i^{(1)}$$



where  $(\theta_i^{(0)}, \tau_i^{(0)})$  and  $(\theta_i^{(1)}, \tau_i^{(1)})$  are phase variables and chiralities before and after the loop update. All the chiralities along the loop are flipped,  $\tau_i^{(1)} = -\tau_i^{(0)}$ , and we can find the updated phase  $\theta_i^{(1)}$  as

$$\theta_i^{(1)} = \theta_i^{(0)} + 2\phi_{i,\text{out}}\tau_i^{(0)}.$$

In total, for each loop  $L$ , we use the following updates for the color configuration,

$$i \in L : \quad \begin{cases} \tau_i^{(0)} & \rightarrow \tau_i^{(1)} = -\tau_i^{(0)}, \\ \theta_i^{(0)} & \rightarrow \theta_i^{(1)} = \theta_i^{(0)} + 2\phi_{i,\text{out}}\tau_i^{(0)}. \end{cases}$$

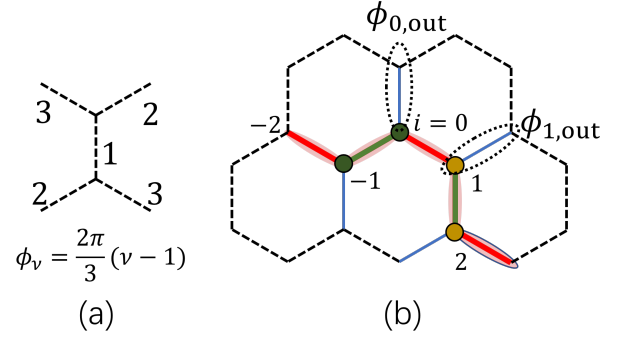


FIG. 5. (a). The three bonds  $\nu = 1, 2, 3$  and the corresponding coupling phase  $\phi_\nu = 0, \frac{2}{3}\pi, \frac{4}{3}\pi$  for them. (b). A schematic diagram for a loop with alternating colors  $RGRG \dots$  and the external bond. The sites  $i$  on the loop are labeled by  $\dots, -2, -1, 0, 1, 2, \dots$ .